Waves in Random and Complex Media
Vol. 00, No. 00, January 2005, 1–18

Frequency shift of sources embedded in finite two-dimensional photonic clusters

A. A. Asatryan,[1] L. C. Botten,[1] N.A. Nicorovici[1],
[1]Department of Mathematical Sciences, University of Technology, Sydney, N.S.W. 2007, Australia,
R. C. McPhedran[2], and C. Martijn de Sterke,[2]
[2]School of Physics, University of Sydney, NSW 2006, Australia
(August 10, 2005)

The frequency (Lamb) shift and local density of states (LDOS) in two-dimensional photonic crystals composed of a cluster of infinitely long circular cylinders is calculated classically using the radiation reaction mechanism. We investigate the frequency shift and LDOS as a function of the size of the cluster and show that, at the edges of the band gap, both quantities can be large and increase in magnitude with cluster size. We explain this in terms of poles of a scattering operator and also show that both the Lamb shift and LDOS are sensitive functions of the shape of the cluster.

1 Introduction

Spontaneous emission [1] and the Lamb (frequency) shift of energy levels of atoms [2] are amongst the fundamental effects observed in quantum electrodynamics. While these were studied originally for atoms in free space, it is now well known that both the emission rate and source frequency can be modified by the environment [3–5]. Such spontaneous emission can be particularly strong in photonic crystals [6], micro-structures with a periodic refractive index distribution, having ranges of propagating states (pass bands) as well as ranges with no propagating states (band gaps) in their frequency spectrum. In infinite photonic crystals, the photon density of states vanishes in band gaps, prohibiting spontaneous emission completely. Accordingly, photonic crystals can be regarded as forming a true vacuum for electromagnetic waves at the gap frequencies. However, when atoms, embedded in a photonic crystal, radiate with a frequency that lies in a band gap but near the gap edge, a variety of interesting, new quantum effects are observed, such as localisation of superradiance near the photonic band edge [7], control of the spontaneous emission rate [8] and non-Markovian character of radiative decay [9, 10].

Calculations of the Lamb shift have been undertaken with different models,

all of which, to date, have assumed that the photonic crystal is infinite. Assuming an isotropic dispersion model, it has been shown that, at the edge of the gap, there exists a photon-atom bound state as well as an enhancement of the Lamb shift [11]. On the other hand, assuming an anisotropic dispersion model, smaller energy shifts (relative to vacuum) have been reported [12]. There also appears to be some controversy concerning the size of the Lamb shift at the edge of the band gap, with Li [13], using a vector model, finding no significant change in the Lamb shift (compared with that observed in free space) for a hydrogen atom embedded in an infinite photonic crystal, and Wang [14] coming to the opposite conclusion.

In reality, all photonic crystals are finite and it is important to understand the effect of both the finite size and cluster shape on the spatial distribution of the Lamb shift—constituting the primary aim of this paper. In our model, we consider a two-dimensional photonic cluster composed of a finite number of cylinders of infinite length, and irradiated with a dipole antenna (line source) which is embedded in the structure. We follow the approach developed by Morawitz *et al* [4] and Kahn *et al* [15] (see also Hinds [16]) for calculating the frequency shifts for a dipole oscillator located near a metallic interface. This treatment was adopted subsequently by Erdogan *et al* [17] to calculate both the frequency shift and the modification of the dumping rate of an embedded line source, and has been successful in explaining experimental observations of Chance *et al* [18]. The frequency shift calculation based on this model can be regarded as an *AC* Stark shift and agrees well with the quantum-mechanically calculated level shift when the source is described by a harmonic oscillator [19].

The results we report here are based on methods similar to those used by us [20–23], who comment on both the 2D Lamb shift (a line source in a cluster of cylinders), and the so-called 2.5D Lamb shift (a point source in a cluster of cylinders). We restrict ourselves to the 2D case, and compare Lamb shifts for both circular and square clusters. The results are surprisingly dissimilar for these two cluster shapes, and we comment on the physics underlying this difference.

The objective of this paper is to investigate the frequency shift and local density of states and their dependence on the size and shape of a photonic crystal cluster, characterising this in terms of poles of a scattering matrix. We begin in Sec. 2 with an outline of the method and present the results and interpretation of our computational simulations in Sec. 3 before giving conclusions in Sec. 4.

2 Model and Method of calculation

2.1 *Frequency shifts*

We begin with a point dipole located at $\boldsymbol{r} = \boldsymbol{r}_s$ in free space—which is equivalent to an infinite line source parallel to the axis of cylinders in three dimensions. The equation of motion for the line source driven by its own radiated field is [4, 15, 17]

$$\frac{d^2p(t)}{dt^2} + \omega_0^2 p(t) = \frac{q^2}{m_0} E_0(\boldsymbol{r}_s, t), \tag{1}$$

where m_0, q and $p(t)$ respectively denote the mass, charge and dipole moment per unit length of the source, and where ω_0 is the frequency of the source when decoupled from all fields. The quantities $p(t)$ and q in turn are related by $p(t) = ql(t)$ where $l(t)$ is the displacement of the electron oscillations, determined by the field amplitude. Here, $E_0(\boldsymbol{r}_s, t)$ is the electric field strength at the location of the dipole. The wave field of the dipole $E_0(\boldsymbol{r}, t)$ is determined by the wave equation

$$\nabla^2 E_0(\boldsymbol{r}, t) + k^2 E_0(\boldsymbol{r}, t) = -\frac{\omega^2 p(t)}{\varepsilon_0 c^2} \delta(\mathbf{r} - \mathbf{r}_s), \tag{2}$$

and has the form

$$E_0(\mathbf{r}, t) = -\frac{\omega^2 p(t)}{\varepsilon_0 c^2} G_0(k|\mathbf{r} - \mathbf{r}_s|), \tag{3}$$

where $G_0(r) = H_0^{(1)}(r)/(4i)$ is the two-dimensional Green function, expressed in terms of the Hankel function of the first kind. Here, ε_0 denotes the free space dielectric permittivity, $k = 2\pi/\lambda$ is the free space wavenumber of the radiation, and c is the speed of light in vacuum. The value of the dipole field $E_0(\boldsymbol{r}, t)$ at the location of the dipole $\mathbf{r} = \mathbf{r}_s$ is infinite and it is necessary to renormalise the mass of the dipole [2]. This renormalisation can be performed classically by noting that the self-reaction damps the oscillations and causes a shift in frequency from ω to ω'. Proceeding in this way [4, 15, 17], we can rewrite the equation of motion (1) in the form

$$\frac{d^2p(t)}{dt^2} + \gamma_0 \frac{dp(t)}{dt} + \omega^2 p(t) = 0, \tag{4}$$

and seek a harmonic time dependent solution of the form $\exp(-i\omega' t)$ which leads to the calculation of the frequency shift

$$\delta\omega = \omega' - \omega. \tag{5}$$

In Eq. (4), ω is the observable frequency and the γ_0 is the damping coefficient which can be calculated as the ratio of the rate of energy radiation P to the total energy of the oscillator W [24],

$$\gamma_0 = \frac{P}{W} = \frac{\omega q^2}{4\varepsilon_0 m c^2}, \tag{6}$$

where P and W are given by

$$P = \frac{q^2 l_0^2 \omega^3}{8\varepsilon_0 c^2}, \quad W = \frac{m\omega^2 l_0^2}{2}. \tag{7}$$

In (7), l_0 denotes the amplitude of the harmonically-varying quantity $l(t)$.

We now generalise the problem from that of an isolated point dipole source to one that is embedded in the two-dimensional cluster of Fig. 1—where the source may be located either in the background medium or in one of the cylinders. This time, the equation of motion of the dipole placed at a point

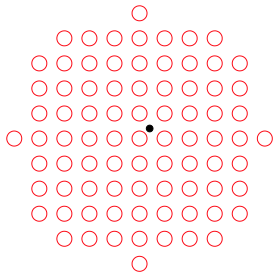

Figure 1. The geometry of the problem.

in the complex multiple scattering environment of the cluster, which is the analogue of Eq. (1), is

$$\frac{d^2 p(t)}{dt^2} + \omega_0^2 p(t) = \frac{q^2}{m_0} E(\boldsymbol{r}_s, t). \tag{8}$$

Here

$$E(\mathbf{r},t) = -\frac{\omega^2 p(t)}{\varepsilon_0 c^2}\left[G_0^{(1)}(k|\mathbf{r}-\mathbf{r}_s|) + G_R(\mathbf{r})\right], \tag{9}$$

is the total field at the location of the dipole, comprising the self field G_0 and the response or scattered (reflected) field G_R. The self reaction field G_0 is again infinite at the location of the dipole and thus requires the renormalisation described above, while the scattered field G_R is finite. The consequence of the self reaction field G_0 is to damp the oscillations, leading to a frequency shift (5). After renormalisation, the equation of motion is

$$\frac{d^2p(t)}{dt^2} + \gamma_0\frac{dp(t)}{dt} + \omega^2 p(t) = -4\omega\gamma_0 p(t) G_R(\mathbf{r}_s). \tag{10}$$

Seeking a harmonic solution $p(t) = pe^{-i\omega' t}$, and noting that $\gamma_0 \ll \omega$, we obtain the shifted frequency

$$\omega' \approx \omega - \frac{\gamma_0^2}{8\omega} + 2\gamma_0 \,\mathsf{Re}\, G_R, \tag{11}$$

and the new damping coefficient

$$\gamma/2 = \gamma_0/2 - 2\gamma_0 \,\mathsf{Im}\, G_R = -2\gamma_0 \,\mathsf{Im}\, G \tag{12}$$

which is proportional to the local density of states (LDOS) [20]. In (11) the term $\gamma_0^2/(8\omega)$ is second order [4, 15, 17] in the small quantity γ, so that the first order frequency shift is

$$\delta\omega = \omega' - \omega \approx -2\gamma_0 \mathsf{Re}\; G_R, \tag{13}$$

and is proportional to the real part of the scattered (response) Green function at the location of the source (11). The new damping coefficient γ is composed of the free space damping coefficient γ_0 and the contribution due to the environment $\gamma_0 \mathsf{Im}\, G_R$, in which the radiated source is located. This damping coefficient γ is also the spontaneous emission coefficient, and from (12) is proportional to the local density of states given by the imaginary part of the Green function [20].

2.2 *Scattered field in a photonic crystal*

For the two-dimensional geometry of Fig. 1 comprising a cluster of N_c cylinders, we use a multipole treatment to calculate the Green function [20], which

is ideally suited to the calculation of the frequency shifts.

For an exterior source, the field in the exterior vicinity of some cylinder l may be expanded in a cylindrical harmonic basis, comprising the regular terms (represented by $J_n(kr)\exp(in\theta)$) sourced by all other cylinders and the exterior source, and the irregular field (represented by $H_n^{(1)}(kr)\exp(in\theta)$) which is sourced on the given cylinder. Equating the local expansion with the global expansion of the type identified by Wijngaard [20] yields a field identity [20], [25, 26] which in matrix form can be written as

$$(\boldsymbol{H}+\boldsymbol{M})\,\boldsymbol{B}=\boldsymbol{Q}. \tag{14}$$

In (14), $\boldsymbol{Q}$ derives from the mutipole representation of the exterior source(s), $\boldsymbol{B}$ is a partitioned vector of multipole coefficients B_m^q for all cylinders, $\boldsymbol{M}$ is a block diagonal matrix containing the boundary condition relations that derive from the continuity conditions, while $\boldsymbol{H}$ is a block partitioned matrix that characterises the interaction of all scatterers in the system, for all scattering orders. By solving this linear system the unknown coefficients can be found and the exterior field may be reconstructed from

$$\begin{aligned} G(\boldsymbol{r},\boldsymbol{r}_s) = {} & \frac{1}{4i}H_0^{(1)}(k|\boldsymbol{r}-\boldsymbol{r}_s|) \\ & + \sum_{q=l}^{N_c}\sum_{m=-\infty}^{\infty} B_m^q H_m^{(1)}(k|\boldsymbol{r}-\boldsymbol{r}_q|)e^{im\arg(\boldsymbol{r}-\boldsymbol{r}_q)}. \end{aligned} \tag{15}$$

while the field interior to cylinder l is reconstructed from

$$G(\boldsymbol{r},\boldsymbol{r}_s)=\sum_{m=-\infty}^{\infty} C_m^l J_m(kn_l|\mathbf{r}-\mathbf{r}_l|)e^{im\arg(\boldsymbol{r}-\boldsymbol{r}_l)}. \tag{16}$$

In the case of a source interior to cylinder l, the interior field is again expanded in the cylindrical harmonic basis, with the regular terms sourced at the cylinder boundary, and with the singular terms associated with the interior source. The exterior form in the vicinity of a particular cylinder has the same form as before, but this time with contributions from only the other cylinders contributing to the regular part of the field. Applying the field continuity conditions at the boundary of the cylinders leads to the field identity, from which the field may be reconstructed everywhere. The exterior form is identical to

that in Eq. (15), but without the source term, while the interior form is now

$$G(\boldsymbol{r},\boldsymbol{r}_s)=\frac{1}{4i}H_0^{(1)}(kn_l|\boldsymbol{r}-\boldsymbol{r}_s|)+\sum_{m=-\infty}^{\infty}C_m^l J_m(kn_l|\mathbf{r}-\mathbf{r}_l|)e^{im\arg(\boldsymbol{r}-\boldsymbol{r}_l)}. \quad (17)$$

The first term in each of Eq. (15) and in Eq. (17) is the unscattered free space dipole field of the oscillator, while the second term is the response (scattered) field of the oscillator $G_R(\boldsymbol{r})$. The frequency shifts are determined by calculating the real part of the reflected field at the location of the oscillator $G_R(\boldsymbol{r}_s,\boldsymbol{r}_s)$, a quantity which is finite and which may be conveniently calculated. Accordingly, the method is both accurate and efficient.

3 Frequency shift and LDOS calculations

In this section we discuss numerical results based on the theory developed in Section 2. In Section 3.1 we present the level shift for clusters of different shapes, and find a very strong dependence on cluster shape. Then in Section 3.2 we show corresponding results for the local density of states. We also discuss the relation between the level shift, local density of states and cluster resonances.

3.1 *Level shift in circular and square clusters*

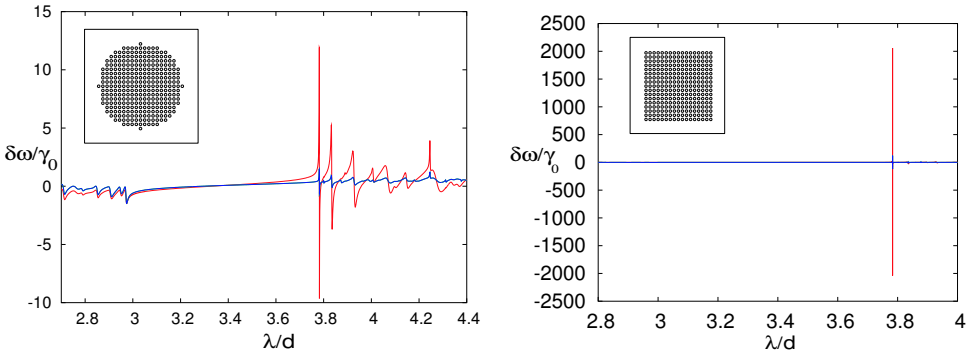

Figure 2. (a) Normalised frequency shift $\delta\omega/\gamma_0$ vs λ/d for a source located at $x=0, y=0$ (red curve) and $x=0, y=0.4$ (blue curve) and for a circular cluster with $N_c=317$; (b) the same as for (a) but for a square cluster of $N_c=289$ cylinders. The insets show the shape of the clusters.

We initially consider a cluster with $N_c=317$ cylinders, each of refractive index $n_l=3$ and radius $a_l=0.3d$, located in air and arranged in a square

lattice, as shown in the insets of Fig. 2 (with d denoting the distance between the neighbouring cylinders). In $E_{\|}$ polarised light, the corresponding infinite structure has a band gap in the wavelength range $2.98 < \lambda/d < 3.769$. Fig. 2(a) displays the radiation shift normalised to the free space radiation rate, $\delta\omega/\gamma_0$, as a function of wavelength for an approximately circular cluster (see inset) at two source locations: inside the central cylinder (red curve) and immediately outside the cylinder (blue curve). It is evident that the frequency shift is enhanced at the long wavelength edge of the band gap at $\lambda/d \approx 3.77$ for points inside the cylinder, and that the shift achieves its most positive value (around 12) at $\lambda/d \approx 3.78176$ and its most negative value (around -9) for $\lambda/d \approx 3.78233$. After these two peaks follow a succession of weaker peaks of alternating sign as the wavelength increases into the lowest-frequency propagating band. In the band gap the radiation shift is small, with weak oscillations apparent just beyond the short wavelength edge of the gap.

Fig. 2(b) displays the normalised frequency shift as a function of wavelength, this time for a cluster of $N_c = 289$ cylinders identical to those for Fig. 2(a) but this time arranged in a square. Here it is evident that the frequency shift is strongly enhanced at the long wavelength edge of the gap at $\lambda/d \approx 3.77$ for points inside of the cylinder, reaching a value of 2×10^3. The maximum frequency shift is $\delta\omega/\gamma_0 = 2058$ occurring at $\lambda/d \approx 3.783142$, with the minimum of $\delta\omega/\gamma_0 = -2038$ occurring at $\lambda/d \approx 3.783147$. These extrema are three order of magnitude higher that the frequency shift for a dipole located near a mirror or between two mirrors [16]. Clearly, from the data in Fig. 2, it is evident that the frequency shift is a strong function of the cluster shape.

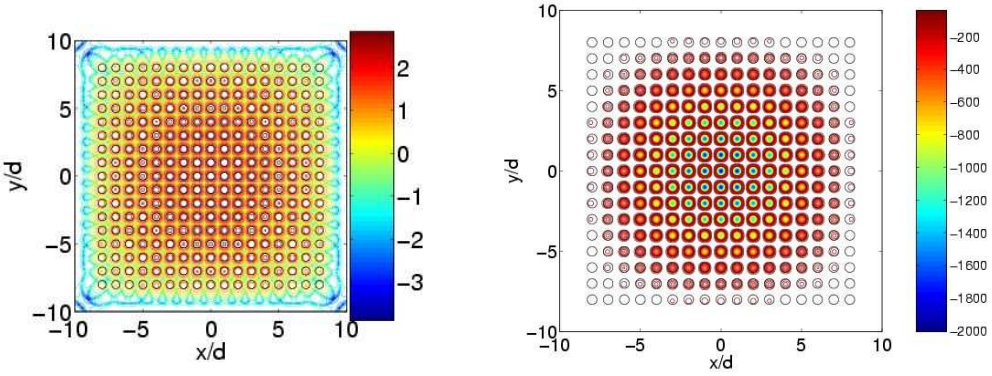

Figure 3. Contour plot of (a) the logarithmic frequency shift $\log_{10}(\delta\omega/\gamma_0)$ in a square cluster for the wavelength $\lambda/d \approx 3.783142$ (b) (linear scale) frequency shift $\delta\omega/\gamma_0$ for $\lambda/d \approx 3.783147$.

In Fig. 3(a) we display $\log_{10}(\delta\omega/\gamma_0)$ as a function of position for a wavelength of $\lambda/d \approx 3.783142$ where the frequency shift is maximal for the square cluster

shown in the inset of Fig. 2(b). Correspondingly Fig. 3(b) shows the map of $\delta\omega/\gamma_0$ (on a linear scale) for the wavelength $\lambda/d \approx 3.783147$ where the frequency shift is minimal $\delta\omega/\gamma_0 = -2038$.

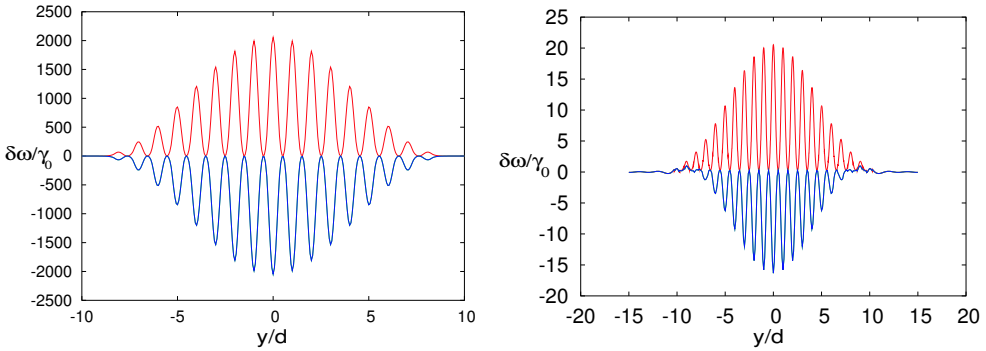

Figure 4. Variation of the frequency shift along the y axis for $\lambda/d = 3.783142$ (red curve) and for $\lambda/d = 3.783147$ (blue curve), for a square cluster with $N_c = 289$ cylinders; (b) the same as for (a) but for a circular cluster with $N_c = 317$ cylinders, red curve is for $\lambda/d = 3.78176$ and blue curve is for $\lambda/d = 3.78233$.

In either case, the magnitude of the frequency shift $|\delta\omega/\gamma_0|$ increases as the centre of the cluster is approached, with the larger shifts occurring for points inside the cylinders. This is clearly seen in Fig. 4 where we plot the variation of the frequency shift along the y axis for the two wavelengths at which the frequency shift is maximal (red curve) and minimal (blue curve). Note the coincidence of the minima and the maxima of the frequency shifts for the two curves in each of Fig. 4(a) and 4(b).

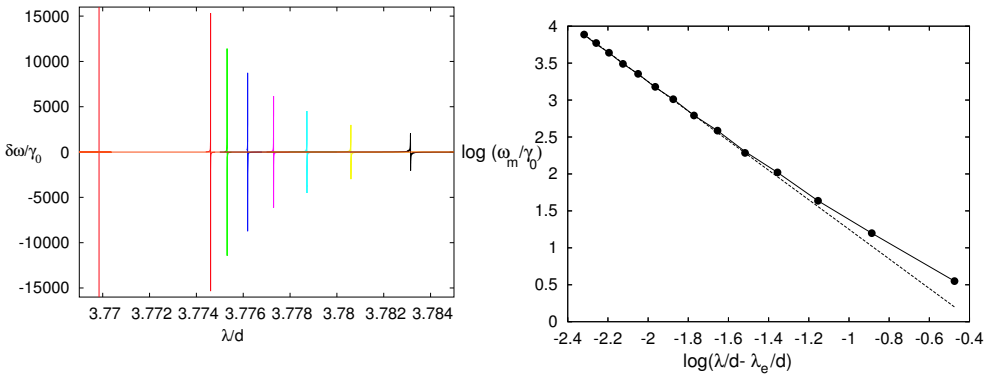

Figure 5. (a) $\delta\omega/\gamma_0$ vs λ/d for square clusters of different size. From right to left, $N_c = 17 \times 17, 19 \times 19, 21 \times 21, 23 \times 23, 25 \times 25, 27 \times 27, 29 \times 29$. The vertical line at $\lambda/d \approx 3.77$ denotes the gap edge; (b) Comparison of the logarithm of the most positive frequency shift vs wavelength (solid line), and a linear fit $\log_{10}(\delta\omega_m/\gamma_0) = -2\log_{10}(\lambda/d - \lambda_e/d) - 0.75$ to the curve (dashed line).

It is also interesting to investigate the dependence of the shift on the size of the cluster. In Fig. 5 we plot the frequency shift versus wavelength for square clusters of different size, with the source located at a common position in the centre of the central cylinder. As is evident from Fig. 5, the frequency shift is a strong function of the size of the cluster. For a cluster comprising 29×29 cylinders, the frequency shift $\delta\omega/\gamma_0$ exceeds 1.5×10^4, four orders of magnitude greater than the corresponding value reported in cavity quantum electrodynamics [16]. Clearly, the size of the frequency shift increases with cluster dimension, with the location of the maxima and minima moving towards the edge of the band gap (associated with the infinite structure) at the wavelength λ_e. The widths of the maxima and minima also decrease as the size of the cluster increases. In Fig. 5(b) we plot the logarithm of the most positive frequency shift $\log_{10}(\delta\omega_m/\gamma_0)$ versus wavelength (solid line), and its linear least squares approximation

$$\log_{10}\left(\frac{\delta\omega_m}{\gamma_0}\right) = -2\log_{10}\left(\frac{\lambda}{d} - \frac{\lambda_e}{d}\right) - 0.75. \tag{18}$$

Fig. 6 displays the dependence on cluster size of the wavelength at which the frequency shift is maximal, together with a nonlinear least squares approximation. The fit is given by the relation

$$\frac{\lambda}{d} = \frac{\lambda_e}{d} + \frac{2.56}{N_c^{0.91}}. \tag{19}$$

From these two fits (Eqns (18) and (19)) we can eliminate $\lambda/d - \lambda_e/d$ and show that $(\delta\omega_m/\gamma_0) \propto N_c^{\alpha}$, with $\alpha \lesssim 2$, a result confirmed by the data.

We next consider the sensitivity of the frequency shift on the shape of the cluster. Fig. 7 displays the frequency shift vs wavelength of the maximal shift for two clusters: (a) a square cluster having 21×21 cylinders (red curve) and (b) a cluster derived from (a) by removing the four corner cylinders (blue curve). The effect of removing the four corner cylinders is dramatic, with the maximum of the frequency shift reducing from $\delta\omega/\gamma_0 = 4528.44$ to $\delta\omega/\gamma_0 = 277.34$ and the location moving by only one part in 10^5 from $\lambda/d = 3.7787197$ to $\lambda/d = 3.7787320$. The width of the maxima and minima are also broadened by the change.

As further confirmation of the sensitivity of frequency shift to cluster shape, we show in Fig. 8 the analogue of Fig.5(a), but now for circular clusters of varying size. Note that the circular cluster never exhibits frequency shifts as large or as rapidly varying as those for the square cluster. Once again, we can see the tendency for the location of the peak of the frequency shift to migrate towards the band edge with increasing cluster size, but for the circular cluster

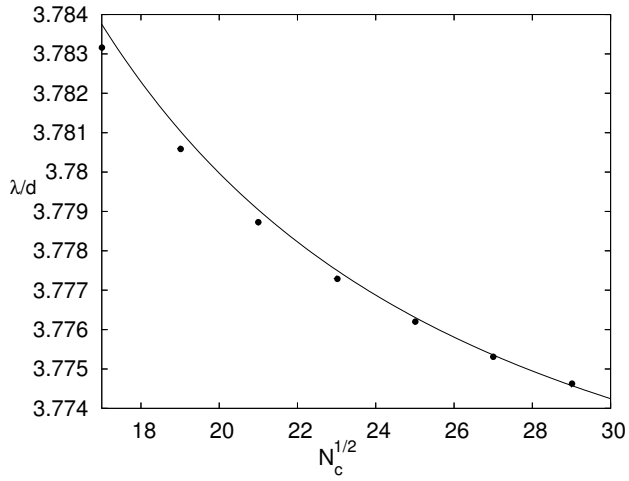

Figure 6. The wavelength λ/d where the frequency shift is maximal vs cluster size N_c (black dots). The curve displays a least squares fit $\lambda/d = \lambda_e/d + 2.56/N_c^{0.91}$ to the data.

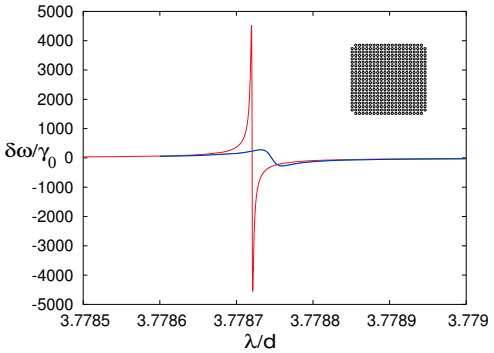

Figure 7. The frequency shift $\delta\omega/\gamma_0$ vs wavelength λ/d for different cluster shapes. The red curve is for a 21×21 square cluster, while the blue curve is for the cluster with the four corner cylinders removed.

there is no sign of the strong increase in magnitude of the frequency shift with size evident in Fig. 5(a). Note that for the latter case, the peak frequency shift scales with cluster size as N_c^α with $\alpha \lesssim 2$.

We have also calculated the frequency shifts for an inverted photonic cluster comprising a hexagonally packed array of circular air voids of common radii $a_l/d = 0.48$ embedded in a dielectric matrix of refractive index $n = 3.605$. In the case of $E_\parallel$ polarisation, the infinite photonic crystal has a band gap in the wavelength range $1.94 < \lambda/d < 2.31$. The results in Fig. 9 display characteristics opposite to those observed for rod-type structures. Specifically, the sharp change of the shift frequency is now located on the short wavelength edge of the gap, while at the long wavelength edge of the gap the shift is

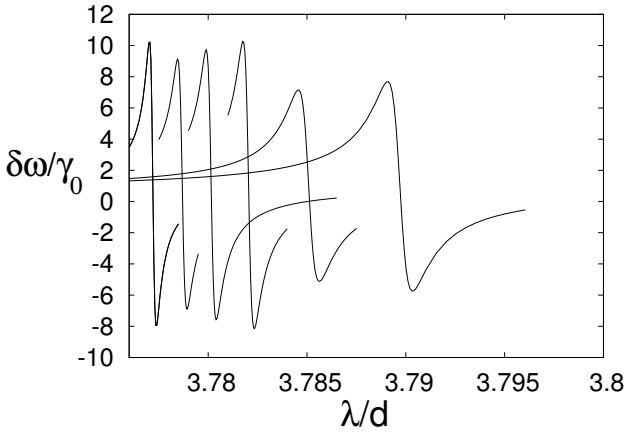

Figure 8. $\delta\omega/\gamma_0$ vs λ/d for circular clusters of different size. From right to left, $D = 17, 19, 21, 23, 25, 27$, where D is the cluster diameter.

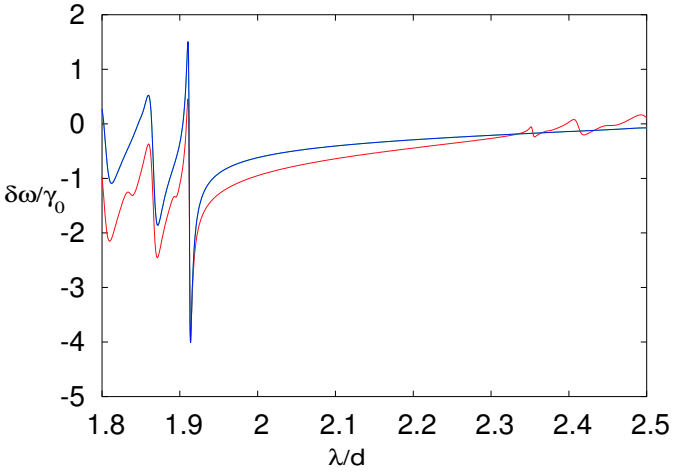

Figure 9. (a) The normalised frequency shift $\delta\omega/\gamma_0$ versus λ/d for source location at $x = 0, y = 0$ (red curve) and $x = 0, y = 0.49$ (blue curve) for a cluster with $N_c = 128$ hexagonally packed cylinders.

substantially weaker.

The strong dependence of the Lamb shift on both wavelength and position in the cluster is amply illustrated in the attached animation which displays contour maps of frequency shift with varying wavelength. The animation spans the first band gap and Fig. 10 depicts a frame comprising a band diagram with a superimposed line showing the normalised frequency for that frame, and a spatial map of the frequency shift coloured according to the legend and scaled according to $(2/\pi)\tan^{-1}(\delta\omega/\gamma_0)$. The animation reveals that the frequency

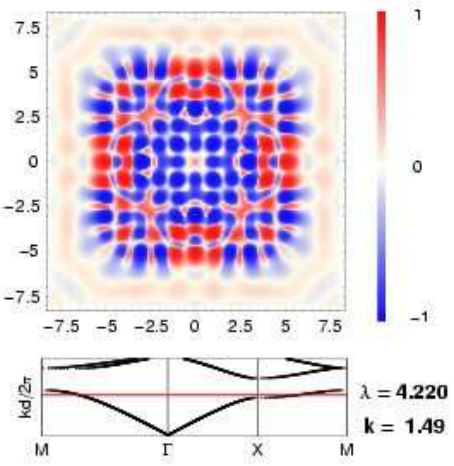

Figure 10. The contour plot of the frequency shift $\log_{10}(\delta\omega/\gamma_0)$ versus position for the wavelength $\lambda/d \approx 4.22$; the dispersion curves of the corresponding infinite structure.

shift is low throughout the cluster for wavelengths shorter than the lower wavelength edge of the gap, but increases monotonically as the wavelength is scanned across the band gap from the short to the long wavelength edges of the gap. Immediately above the long wavelength edge of the gap (in the pass band) there is a sharp increase in the Lamb shift throughout the cluster, followed by a sequence of complex patterns with increasing wavelength, similar to resonances in Fig. 2(a) in the long wavelength pass band.

The influence of the shape of the cluster may be understood in terms of Fabry-Perot resonances that enhance the Lamb shift. Exemplifying this is the much stronger shift that is apparent for the square array than is observed for either the circular cluster or the square cluster with its corner cylinders removed. We have also calculated the frequency shifts for rectangular clusters with high aspect ratio and observed a similar behaviour for the frequency shift as for square clusters. All of this supports the interpretation that substantial frequency shifts rely on strong resonance effects generated by multiple reflections from ideal mirror boundaries, with the width of the resonance decreasing with increasing cluster size, as in Fabry-Perot interferometers.

Given that the behaviour of the square clusters are similar to the rectangular clusters we consider a one dimensional model to demonstrate the Fabry-Perot interpretation. In this model we impose quasi-periodicity along the x axis and have a finite number of identical layers in the y direction. The central layer has a point source embedded in the cylinder and there are N_L layers of gratings on each side of the central grating (see Fig.11). We embed an array of quasiperiodically phased sources in the cylinders of the central grating and then by integration of the solutions of the family of different problems

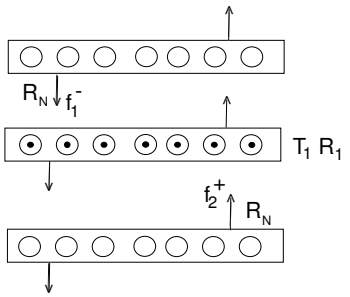

Figure 11. The quasi one-dimensional model.

over the 1st zone, we may calculate the Green's function corresponding to a single source in the central cylinder of the central grating (for the details see Ref. [27]). The field at the central cylinder is driven by the incoming plane wave fields from below $\mathbf{f}_2^+$ and from above $\mathbf{f}_1^-$ and we can show that the total incident field that drives the central grating can be written as

$$\boldsymbol{f}_1^- + \boldsymbol{f}_2^+ = (\boldsymbol{I} - \boldsymbol{L}\boldsymbol{T}_1)^{-1}\boldsymbol{L}\boldsymbol{Q}_t, \tag{20}$$

$$\boldsymbol{L} = \boldsymbol{R}_N(\boldsymbol{I} - \boldsymbol{R}_1\boldsymbol{R}_N)^{-1}, \tag{21}$$

using a derivation related to that given in [27]. Here $\boldsymbol{R}_1$ and $\boldsymbol{T}_1$ are plane wave reflection and transmission matrices for a single layer and $\boldsymbol{R}_N$ is the plane wave reflection matrix for an N layer grating, while $\boldsymbol{Q}_t$ is a vector containing the plane wave coefficients corresponding to a point source transmitted through the cylinder above and below the grating. This expression (21) quantifies the Fabry-Perot interpretation, with the term $(\boldsymbol{I} - \boldsymbol{L}\boldsymbol{T}_1)^{-1}$ characterising the resonance. Numerical experiments show that the primary resonance increases in shape and moves towards the edge of the gap as the number of layers increases, corresponding the reflectance of the bulk slab approaching unity as the band gap edge is approached.

3.2 *Local Density of States*

We turn now to consider analogous LDOS properties and note that in earlier work [25, 26] we investigated its behaviour as a function of cluster size, for an approximately circular cluster. Given that the frequency shift is shown to be a strong function of the size of the cluster, one would expect that the LDOS would increase as a function of cluster size, given the Hilbert transform connection between LDOS and frequency shift [14,23,28] for infinite structures. Fig. 12(a) plots the LDOS as a function of wavelength close to the gap edge for square clusters of dimension 17×17 (blue curve), 19×19 (green curve) and $21\times$

21 (red curve). In all cases the LDOS is a very sharp function of wavelength, with the maximum value increasing from $\gamma/(4\gamma_0) = 2016$ at wavelength $\lambda/d = 3.783140$ to the value $\gamma/(4\gamma_0) = 4526$ at $\lambda/d = 3.7787205$. Also, the width of the peak decreases with increasing cluster size, with the area under the curve preserved to within approximately 15%. Because of the sharpness of the features in Fig. 12(a), we replot both the LDOS and the corresponding frequency shift in Fig. 12(b) on an expanded wavelength scale.

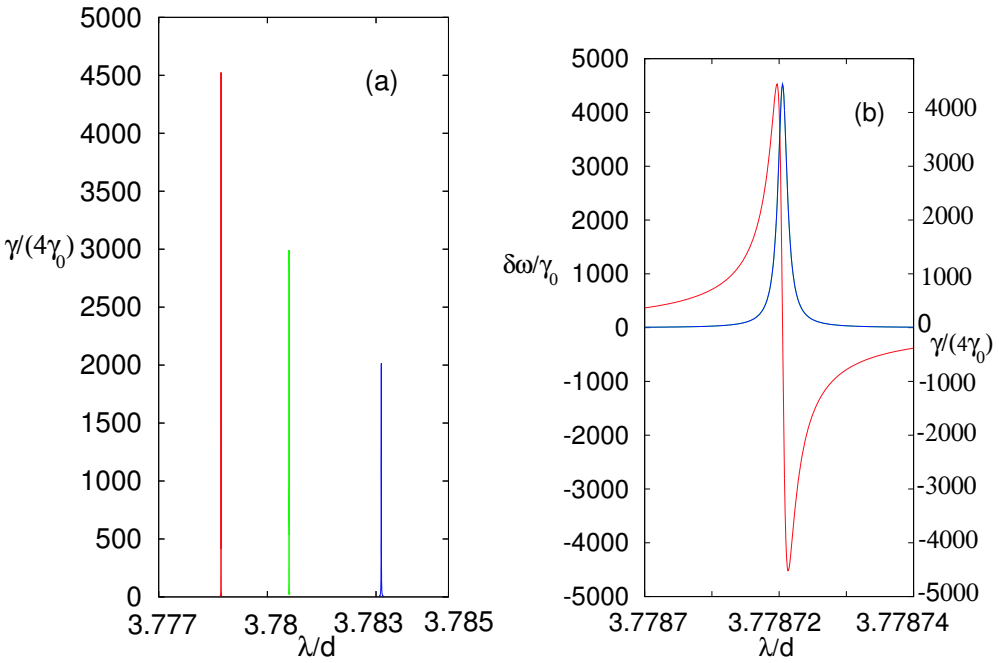

Figure 12. (a) LDOS vs wavelength for clusters of different sizes: 17×17 (blue curve), 19×19 (green curve) and 21×21 (red curve). (b) Plots of the frequency shift $\delta\omega/\gamma_0$ vs wavelength (red curve and left axis label) and LDOS $\gamma/4\gamma_0$ vs wavelength (blue curve and right axis label) for a square 21×21 cluster.

From Fig. 13, which shows the variation of LDOS with wavelength for a square cluster (red line) and a derived cluster with the four corner cylinders removed, it is clear that the LDOS behaves in an analogous manner to the frequency shift and is a very sensitive function of shape. The maximum value of the LDOS decreases sharply, by an order of magnitude, from the maximum value 4500 to a value below 500, while the resonance width also broadens as we remove cylinders.

The strongly resonant behaviour that is exhibited by both the frequency shift and the LDOS is determined by the structure of the poles of the scattering operator $\boldsymbol{S} = (\boldsymbol{H} + \boldsymbol{M})^{-1}$ that derives from the field identity (14). At the band

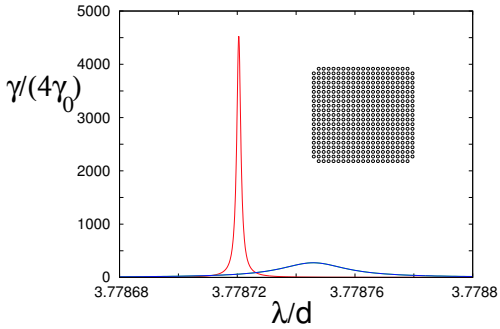

Figure 13. LDOS as a function of wavelength near the band gap edge. The red curve is for a 21×21 square cluster, while the blue curve is for a cluster derived from the former by removing the four corner cylinders (see inset).

edge, the poles of the scattering matrix (i.e., points such that $\det(\boldsymbol{S}) = 0$) tend to lie close to the real axis, thus generating a stronger response field that leads to enhanced resonances. In Fig. 14(a) we plot the location of the poles in the complex wavelength plane λ/d for clusters of sizes 17×17, 19×19, 21×21, 23×23 and 25×25. As the size of the cluster increases, we see that the poles move towards the real axis, sharpening the features exhibited in both the frequency shift and LDOS calculations. Note that for an infinite photonic crystal, the pole will be located precisely on the real axis, and will correspond to a mode of the periodic structure occurring in a band diagram.

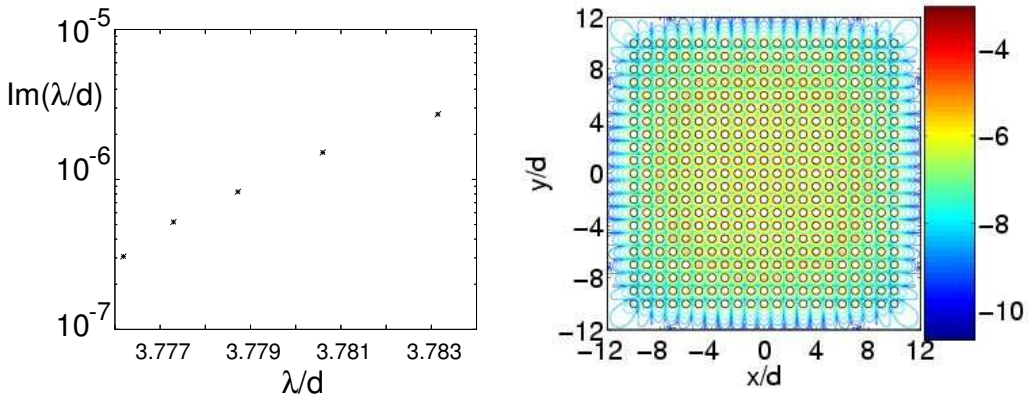

Figure 14. (a) The location of the poles in the complex λ/d plane for a clusters of sizes 17×17, 19×19 , 21×21 , 23×23, and 25×25 from right to left; (b) spatial distribution of the logarithm of modal intensity $\log_{10} |E|^2$ for the 21×21 cluster.

In Fig. 14(b) we plot the spatial distribution of the mode intensity for a 21×21 cluster, corresponding to the third point from the left in Fig. 14(a).

The intensity of this mode is maximal inside the cylinders and is associated with the dielectric band mode of the corresponding infinite photonic crystal. The quality factor of this mode can be estimated from the imaginary part of the wavelength, which gives $Q = \lambda'/(2\lambda'') = 2.28 \times 10^6$, where $\lambda = \lambda' + i\lambda''$. The high quality factor and the distribution of the mode implies that the mode has a long lifetime and is thus capable of interacting strongly with the emitter, giving rise to strong sharp features in both the frequency shift and LDOS.

4 Conclusion

We have calculated the radiation frequency shift and LDOS of a line source located inside a two-dimensional photonic crystal composed of a finite cluster of cylinders with infinite length and have found that both the frequency shift and the LDOS are strongly enhanced at the edges of the band gap. The value of the frequency shift can be either positive or negative and the magnitude of both the frequency shift and the LDOS is a highly sensitive function of wavelength and cluster shape. Both the LDOS and frequency shift increase strongly with size for square and rectangular clusters. In fact, frequency shifts which are four orders of magnitude higher than reported in cavity quantum electrodynamics [16] are observed. Despite such strong enhancement, the measurement of the frequency shift in the visible and near infrared may be experimentally challenging, given that disorder and absorption are likely to adversely affect the enhancement of the frequency shift. Furthermore, the spectral width of the enhanced Lamb shift and LDOS can be very narrow and may not be easy to locate. Microwave experimental verification of the predictions made here would be valuable.

As argued earlier, the substantial radiation effects we have demonstrated are caused by strong resonances arising from multiple reflections within square and rectangular clusters. Given that these resonance are so narrow, it is not surprising that apparent small changes to the geometry substantially degrade the quality of the resonator. The extraordinary sensitivity of frequency shift to cluster shape we have exhibited here warrants further investigation.

The computational approach that has been adopted here is also applicable to $3D$ problems, and indeed, the extent to which the results of this 2D study carry over into 3D will make for an interesting extension of this study.

Acknowledgment Support from the Australian Research Consul is acknowledged.

References

[1] Weisskopf, V.F. and Wigner, E., 1930, Z. Phys. **63**, 54.
[2] Bethe, H.A., 1947, The electromagnetic shift of energy levels. *Phys. Rev.* **72**, 339-341.
[3] Purcell, E.M., 1946, Spontaneous emission probabilities at radio frequencies, *Phys. Rev.*, **69**, 681.
[4] Moravitz, H., 1969, Self-coupling of a two-level system by a mirror. *Phys. Rev.* **187***, 1792-1796.*
[5] Kleppner, D.,1981, Inhibited spontaneous emission. *Phys. Rev. Lett.* **47**, 233-236.
[6] Joannopoulos, J.D., Meade, R.D. and Winn J.N., 1995, *Photonic Crystals*, (Princeton, Princeton University Press).
[7] John, S., Quang, T., 1995, Localization of superradiance near photonic band edge. *Phys. Rev. Lett.* **74**, 3419-3422.
[8] Quang, T., Woldeyohannes, M., John, S. and Agarwal, G.S., 1997, Coherent control of spontaneous emission near a photonic band edge: a single atom memoty device. *Phys. Rev. Lett.*, **79**, 5238-5241.
[9] Kofman, A.G., Kurizki, G., and Sherman, B., 1994, Spontaneous and induced atomic decay in photonic band structures. *J. Mod. Opt.* **41** 353-384.
[10] Busch, K., Vats, N., John, S., and Sanders, B.C., 2000, Radiating dipoles in photonic crystals, *Phys. Rev. E* **62**, 4251-4260.
[11] John, S. and Wang, J., 1990, Quantum Electrodynamics near a Photonic Band Gap: photon bound states and dressed atoms. *Phys. Rev. Lett.* **64**, 2418-2421.
[12] Zhu, S.-Y., Yang, Y., Chen, H., Zheng, H. and Zubairy, M.S., 2000, Spontaneous radiation and lamb shift in three-dimensional photonic crystals. *Phys. Rev. Lett.* **84**, 2136-2139.
[13] Li, Z.-Y. and Xia, Y., 2001, Optical photonic band gaps and lamb shift. *Phys. Rev. Lett.* **63**, 121305:1-4.
[14] Wang, X.-H., Kivshar, Y.S. and Gu, B.Y., 2004, Giant Lamb shift in photonic crystals. *Phys. Rev. Lett.*, **93** 073901-1:4.
[15] Kahn, H., 1969, Classical aspect of energy transfer in molecular systems. *J. Chem. Phys.* **53**, 101-108.
[16] Hinds, E.A., 1994, In: P.R. Berman (Ed.) *Cavity quantum electrodynamics* (Boston, Academic Press).
[17] Erdogan, T., Sullivan, K.G. and Hall, D.G., 1993, Enhuncement and inhibition of radiation in cylindrically symmetric, periodic structures. *J. Opt. Soc. Am. B* **10**, 391-398.
[18] Chance, R.R., Prock, A. and Silbey, R., 1975, Frequency shifts of an electric-dipole transition near a partially reflecting surface. *Phys. Rev. A* **12**, 1448-1452.
[19] Wylie, J.M. and Sipe, J.E., 1985, Quantum electrodynamics near an interface. II. *Phys. Rev. A*, **32**, 2030-2043.
[20] Asatryan, A.A., Fabre, S., Busch, K., McPhedran, R.C., Botten, L.C., de Sterke, C.M. and Nicorovici, N.A., 2001, Two-dimensional local density of states in two-dimensional photonic crystals. *Opt. Exp.*, **8**, 191-197.
[21] Asatryan, A.A., Botten, L.C., Langtry, T.N., Fussell, D., McPhedran, R.C., and de Sterke, C.M., Lamb shift of sources in two-dimensional photonic crystals, ACOFT/AOS Conference Proceedings CD-ROM ISBN 0-7315-5222-9, Canberra, 5-8 July, (2004).
[22] D. Fussell, R.C. McPhedran, C.M. de Sterke, Decay rate and level shift in a circular dielectric waveguide, Phys. Rev. A **71**, 013815 (2005).
[23] D. Fussell, R.C. McPhedran, C.M. de Sterke, Phys. Rev. E, Two-dimensional treatment of the decay rate and level shift in photonic crystals, submitted. (2005)
[24] Feynman, R., Leighton, R. and Sands M., 1977, *The Feynman Lectures on Physics, II,* (NY, Addison-Wesley).
[25] Asatryan, A.A., Busch, K., McPhedran, R.C., Botten, L.C., de Sterke, C.M. and Nicorovici, N.A., 2001, Two-dimensional local density of states in two-dimensional photonic crystals. *Phys. Rev. E*, **63**, 046612.
[26] Asatryan, A.A., Busch, K., McPhedran, R.C., Botten, L.C., de Sterke, C.M. and Nicorovici, N.A., 2001, Two-dimensional Green tensor and local density of states in finite-sized two-dimensional photonic crystals, 2003, *Waves in Random Media*, **13**, 9-25.
[27] Wilcox S., Botten L.C., McpPhedran, R.C., Poulton C.G., and C. Martijn de Sterke, 2005, Modelling of the defect modes in photonic crystals using the fictitious source superposition method, *Phys. Rev. E* **71**, 056606.
[28] Cohen-Tannoudji, C., Dupont-Poc, J., and Grynberg, G., 1992, *Atom-Photon Interactions. Basic Processes and Application* (NY John Wiley & Sons).